ADVANCES IN CHEMICAL PHYSICS—VOLUME L

I. Prigogine and Stuart A. Rice—Editors

DYNAMICS OF THE EXCITED STATE

Edited by

K. P. LAWLEY

Department of Chemistry
University of Edinburgh

AN INTERSCIENCE® PUBLICATION

JOHN WILEY & SONS

CHICHESTER · NEW YORK · BRISBANE · TORONTO · SINGAPORE

ADVANCES IN CHEMICAL PHYSICS

VOLUME L

SERIES EDITORIAL BOARD

ADVANCES IN CHEMICAL PHYSICS—VOLUME L

I. Prigogine and Stuart A. Rice—Editors

DYNAMICS OF THE EXCITED STATE

Edited by

K. P. LAWLEY

Department of Chemistry
University of Edinburgh

AN INTERSCIENCE® PUBLICATION

JOHN WILEY & SONS

CHICHESTER · NEW YORK · BRISBANE · TORONTO · SINGAPORE

British Library Cataloguing in Publication Data:

Dynamics of the excited state,
— (Advances in chemical physics; v. 50)
1. Molecules
2. Excited state chemistry
I. Lawley, K. P. II. Series
541.2'8 QD461.5

ISBN 0 471 10059 5

Photosetting by Thomson Press (India) Limited, New Delhi
Printed by The Pitman Press, Bath.

INTRODUCTION

Few of us can any longer keep up with the flood of scientific literature, even in specialized subfields. Any attempt to do more, and be broadly educated with respect to a large domain of science, has the appearance of tilting at windmills. Yet the synthesis of ideas drawn from different subjects into new, powerful, general concepts is as valuable as ever, and the desire to remain educated persists in all scientists. This series, *Advances in Chemical Physics*, is devoted to helping the reader obtain general information about a wide variety of topics in chemical physics, which field we interpret very broadly. Our intent is to have experts present comprehensive analyses of subjects of interest and to encourage the expression of individual points of view. We hope that this approach to the presentation of an overview of a subject will both stimulate new research and serve as a personalized learning text for beginners in a field.

ILYA PRIGOGINE

STUART A. RICE

CONTRIBUTORS TO VOLUME L

W. H. BRECKENRIDGE, Department of Chemistry, University of Utah, Salt Lake City, UT 84112, USA

T. A. BRUNNER, Research Laboratory of Electronics and Department of Physics, Massachusetts Institute of Technology, Cambridge, MA 02139, USA

M. A. A. CLYNE deceased, formerly Department of Chemistry, Queen Mary College, Mile End Road, London E1 4NS, UK

I. V. HERTEL, Institut für Molekülphysik, Fachbereich Physik der Freien Universität Berlin, Boltzmannstrasse 20, 1000 Berlin 33, West Germany

D. M. HIRST, Department of Chemistry and Molecular Sciences, University of Warwick, Coventry CV4 7AL, UK

D. S. KING, National Bureau of Standards, Division of Molecular Spectroscopy, Washington, DC 20234, USA

A. M. F. LAU, Corporate Research Science Laboratories, Exxon Research and Engineering Company, PO Box 45, Linden, NJ 07036, USA

S. R. LEONE, Joint Institute for Laboratory Astrophysics, National Bureau of Standards and University of Colorado; and Department of Chemistry, University of Colorado, Boulder, CO 80309, USA

I. S. MCDERMID, Molecular Physics and Chemistry Section, Jet Propulsion Laboratory, California Institute of Technology, 4800 Oak Grove Drive, Pasadena, CA 91109, USA

D. PRITCHARD, Research Laboratory of Electronics and Department of Physics, Massachusetts Institute of Technology, Cambridge, MA 02139, USA

M. QUACK, Institut für Physikalische Chemie der Universität, Tammannstrasse 6, D-3400 Göttingen, West Germany

H. UMEMOTO, Department of Chemistry, University of Utah, Salt Lake City, UT 84112, USA

CONTENTS

Dynamics of the Excited State
Edited by K. P. Lawley

LASER-INDUCED FLUORESCENCE: ELECTRONICALLY EXCITED STATES OF SMALL MOLECULES

THE LATE MICHAEL A. A. CLYNE

Department of Chemistry, Queen Mary College, Mile End Road, London E1 4NS, UK

AND

I. STUART McDERMID

Molecular Physics and Chemistry Section, Jet Propulsion Loboratory, California Institute of Technology, 4800 *Oak Grove Drive, Pasadena, CA* 91109, *USA*

CONTENTS

I. INTRODUCTION

The frequency of laser radiation may be tuned into coincidence with an absorption line of an atom or molecule. The resulting emission of radiation from the upper state of the transition is termed laser-induced fluorescence (LIF), and it provides a highly sensitive and specific means of detecting species in their ground states. Thus, LIF is very useful, for example, in the kinetic studies by Baronavski *et al.* (1978) of metastable-excited ground-state species, and as an analytical method of measuring small concentrations of certain trace species such as HCHO (Becker *et al.*, 1975) and OH (Wang and Davis, 1974; Davis *et al.*, 1979) radicals in the atmosphere. Suitable species for LIF studies are those whose excited electronic states are stable, i.e. not predissociated, and which possess intense transitions in an appropriate energy region.

When reasonably narrow-band excitation ($\leqslant 10\,\text{GHz}$) is used, LIF with dye lasers provides a means of determining vibrational and rotational populations in molecules. Following the pioneering work of Zare and his colleagues (Cruse *et al.*, 1973; Zare and Dagdigian, 1974; Zare, 1979), highly detailed and elegant studies are being carried out of initial energy distributions in molecules formed in elementary reactions. Many of these investigations are being undertaken under molecular beam conditions, in order to provide well determined collisions.

Application of LIF specifically to the identification of photofragments in beam experiments is another extremely promising application, which is discussed in the article by Leone in this volume. LIF provides a direct method of studying the dynamics of excited states. In these studies, a short (nanosecond) pulse of laser radiation is used to form the excited electronic state. The decay of fluorescence from the excited state is then measured in real time, giving kinetic information about collision-free or collisional elementary processes. Modern techniques for the direct study of fluorescence decay and the measurement of lifetimes and relaxation rate constants have recently been reviewed by McDermid (1981). Radiative and predissociative lifetimes may be determined, whilst collisional data of significance include the rate constants for electronic quenching, ro-vibrational energy transfer and collisional predissociation. Examples of species that have been studied in this way include the $B^3\Pi(0^+)$ states of halogens and interhalogens (Clyne

and McDermid, 1978a), the OH radical (German, 1975a, b, 1976; McDermid and Laudenslager, 1980) and SO (Clyne and McDermid, 1979e) free radicals. It is a great simplification that initial excitation can be confined to a single ro-vibrational state (v', J') of a diatomic molecule, when lasers with relatively narrow bandwidths ($\leqslant 3$ GHz) are used. Thus it is possible to determine state-to-state rate constants in work of this type.

Before considering laser-induced fluorescence for molecules in more detail, it is useful first to review briefly the conceptually simpler technique of atomic resonance fluorescence.

A. Atomic Resonance Fluorescence

The use of resonance fluorescence as a method of detecting atoms in defined quantum states was established many years ago, and was reviewed by Mitchell and Zemansky (1934) in their wellknown monograph *Resonance Radiation and Excited Atoms*. An atomic resonance line from a suitable lamp (e.g. Na) is absorbed by ground-state atoms, the subsequent re-emission of radiation being an extremely sensitive and specific indicator of the atoms in question. Quantitative calibration of the fluorescence intensity in terms of atom concentration was seldom achieved in earlier work, because the intensities of absorption and fluorescence are dependent on the lineshape of the emitter in the lamp, and on that of the absorbing atoms. The absorber normally has a well defined lineshape, which is typically a Doppler, Gaussian profile at low pressures. However, the lamp emitter normally is strongly self-reversed and has a translational temperature that is not well defined but is above 300 K; values of 500–1000 K are typical for a low-power (50 W) microwave discharge operating at 2·45 GHz.

Recently, atomic resonance fluorescence has been developed as a quantitative method of measuring atom concentrations (Braun and Carrington, 1969; Anderson and Kaufman, 1972; Clyne and Nip, 1979). The use of a tunable dye laser exhibiting narrow bandwidth has obvious advantages over the earlier resonance lamps. When a continuous-wave (CW) dye laser is set up with several intracavity etalons, the laser oscillates on a single longitudinal mode whose bandwidth is much less than the Doppler linewidth (-3 GHz) of a typical atom or molecule at 300 K (Schafer, 1973). With stabilization of laser frequency and intensity, extremely low sodium atom concentrations (< 1 atom cm^{-3}) can be detected at 570 nm (Kuhl and Marowsky, 1971). In addition, the narrow bandwidth of CW dye lasers has opened up a vast new field of sub-Doppler atomic spectroscopy that encompasses the various types of hyperfine splitting of energy levels. This field has been reviewed in books edited by Walther (1976) and by Shimoda (1976) and will not be covered in the present work.

Unfortunately, the scope for detecting a variety of atoms using laser

resonance fluorescence is rather limited. This limitation arises from the restricted range of wavelengths available from dye lasers, particularly from CW dye lasers which operate most easily at wavelengths above 550 nm. Pulsed dye lasers are more useful, since their fundamental wavelength ranges extend routinely below 400 nm, and frequency doubling or frequency mixing leads to usable ultraviolet (UV) energies below 260 nm; see, for example, Byer and Herbst (1978) and Byer (1980).

For the detection of most non-metallic atoms, resonant radiation in the vacuum ultraviolet spectrum ($\lambda < 200$ nm) is required. Lasers capable of operating in this wavelength region are beginning to become available, and two-photon excitation with conventional UV photons has been demonstrated by Hansch *et al.* (1975) for the $1s$–$2s$ transition of H near 121·6 nm. However, at the present time, conventional microwave-excited resonance lamps are used routinely to follow concentrations of common non-metallic atoms, such as H, O, N, Cl, Br, S, and I. This approach has led to a method of studying the kinetics of atomic reactions, which has been extremely fruitful in leading to many hitherto unknown rate constants; for a review, see Baulch *et al.* (1980). Kinetic uses of atomic resonance fluorescence in the vacuum ultraviolet, and the closely related resonance absorption have been reviewed recently by Clyne and Nip (1979) and by Donovan and Gillespie (1975).

B. Linewidth Considerations

Factors influencing achievable signal-to-noise ratio are common to atoms and molecules, although additional factors are introduced in the consideration of molecular fluorescence. We consider initially the influence of linewidth on atomic fluorescence using radiation in the visible and ultraviolet range. At low pressures (~ 1 Torr or less) and at temperatures $T \geqslant 100$ K, the line profile of an absorbing atom is determined almost entirely by the Doppler width $\Delta\nu_D$, given by (Mitchell and Zemansky, 1934)

$$\Delta\nu_D = 2\nu_D 2R \ln 2 (T/M)^{1/2}/c. \tag{1.1}$$

(This will not necessarily be the case for infrared fluorescence, for which the magnitude of $\Delta\nu_D$ is much less than for ultraviolet visible radiation. Thus, the lineshape for absorption of infrared radiation tends towards a Lorentzian whose linewidth is determined by the radiative lifetime and by pressure broadening even in the torr pressure range.)

The Doppler line appropriate to absorption of ultraviolet/visible radiation has a Gaussian form given by

$$k_\nu = k_0 \exp(-\omega^2). \tag{1.2}$$

In Eq. (1.2), k_ν is the absorption coefficient at frequency ν and k_0 is the absorption coefficient at the line centre; ω is a reduced-frequency function

given by

$$\omega = 2(\ln 2)^{1/2}(\nu - \nu_0)/\Delta\nu_D. \tag{1.3}$$

Clearly, the absorption of energy is maximized when the linewidth of the incident radiation $\Delta\nu_s$ is equal to or less than the magnitude of $\Delta\nu_D$. Use of an extremely narrow linewidth, for example a few megahertz such as is available from a stable single-mode dye laser, may not be favourable. It is possible to burn out the centre of the absorption line so that no population remains in the lower state.

The case where $\Delta\nu = \Delta\nu_D$ is simple; also, it frequently approximates to the practical linewidth of an etalon-narrowed, pulsed dye laser. We assume optically thin conditions, i.e. when $I_{abs}/I_0 \to 0$, and a Doppler profile for the exciting radiation. Both assumptions will usually be good approximations. The expression for the integrated energy absorbed in a Doppler line is given approximately (Mitchell and Zemansky, 1934; Bemand and Clyne, 1973)

$$I_{abs}/I_0 \simeq k_0 l/(1+\alpha^2)^{1/2}, \tag{1.4}$$

where l is the absorbing pathlength and $\alpha = \Delta\nu_s/\Delta\nu_D$. For equal linewidths of emitter and absorber, $\alpha = 1$; and thus

$$I_{abs}/I_0 = 0.7 k_0 l. \tag{1.4a}$$

Eq. (1.4) implies a proportional dependence of I_{abs}/I_0 upon absorber concentration N (Bemand and Clyne, 1973) since, for atomic absorption in the Doppler model, k_0 is proportional to N through

$$k_0 = 2fN[(\ln 2)/\pi]^{1/2}(\pi e^2/mc)\Delta\nu_D. \tag{1.5}$$

In Eq. (1.5), f is the atomic oscillator strength of the relevant transition.

When $I_{abs}/I_0 \gg 0$, optically thin conditions do not prevail and the dependence of I_{abs}/I_0 upon N becomes nonlinear. Curves of growth, relating I_{abs}/I_0 to N for simple cases, have been given by Mitchell and Zemansky (1934), Braun and Carrington (1969), and Bemand and Clyne (1973).

C. Oscillator Strength and Lifetime of an Atomic Transition

Eq. (1.5) indicates that k_0, the absorption coefficient at the line centre, is directly proportional to the oscillator strength f of the relevant atomic transition. Thus, the fluorescence intensity varies in direct proportion with f, assuming optically thin fluorescence. A similar conclusion is also valid for molecular fluorescence.

A number of different quantities are used to describe the probability of an electronic transition. In atomic spectroscopy, the oscillator strength f is commonly used. In molecular spectroscopy, various quantities are used, of which we select the electric dipole moment $|R_e|^2$ as one of the more

fundamental parameters describing a transition probability. The magnitudes of f and $|R_e|^2$ are related in a relatively simple manner to absorption intensity, as for example through Eqs. (1.4) and (1.5) for atomic absorption.

The radiative lifetime of the upper state τ_R is clearly related closely to emission phenomena, such as the measured excited-state lifetimes. The value of τ_R^{-1} measures the sum of Einstein coefficients for all spontaneously emitting processes out of the upper state. Thus, if the branching ratio out of the upper state is known, τ_R can be related to f or to $|R_e|^2$ for a particular transition. For an atomic transition such that g_1 and g_2 are the statistical weights of the ground and excited states, the relevant relationship (Mitchell and Zemansky, 1934) is

$$\tau_R^{-1} = (8\pi^2 e^2 \nu_0^2/mc^3)(g_1/g_2)f. \tag{1.6}$$

D. Electric Dipole Moment and Lifetime of a Molecular Transition

The radiative lifetime for a molecular electronic transition is related to the corresponding electric dipole moment through (Zaraga *et al.*, 1976; Okabe, 1978)

$$\tau_R^{-1} = (64\pi^4/3h)\sum_{v''} |R_e|^2 q_{v',v''} \nu^3. \tag{1.7}$$

In Eq. (1.7), $q_{v',v''}$ is the Franck–Condon density for a particular vibrational transition v'–v'' at frequency ν. The summation in Eq. (1.7) represents the fact that emission out of the initial state v' is distributed amongst a number of ground-state v'' levels, according to the Franck–Condon densities.

Eq. (1.7) cannot be solved to give a single value of $|R_e|^2$ from a measured value of τ_R, since it allows for the fact that $|R_e|^2$ can vary with v'', and thus with the r-centroid $\bar{r}$ of the transition. Often, the variation of $|R_e|^2$ over a limited range of $\bar{r}$ is small. The Eq. (1.7) may therefore be simplified by assuming a constant value of $|R_e|^2$, as in Eq. (1.8) (Zaraga *et al.*, 1976; Okabe, 1978)

$$\tau_R^{-1} = (64\pi^4/3h)|R_e|^2(\bar{\nu})^3. \tag{1.8}$$

$(\bar{\nu})^3$ is defined as

$$(\bar{\nu})^3 = \sum_{v''} \nu^3 q_{v',v''}.$$

Substitution of the measured value for τ_R then leads directly to a mean value of $|R_e|^2$, averaged over the range of r-centroids of importance in the transition.

The accuracy of this approach is dependent upon the availability of reliable Franck–Condon densities. For many molecules, such as the halogens (Coxon, 1971), interhalogens (Clyne and McDermid, 1976a), OH (Crosley and Lengel, 1975; Chidsey and Crosley, 1980), CN (Rao and Lakshman, 1972), etc.,

accurate RKR potential energy curves and the derived Franck–Condon densities are now available over considerable ranges of v' and v''. However, for other molecules, the spectroscopic data base is insufficient, and relatively unreliable Franck–Condon densities based on Morse potential energy curves only are available. It is important, therefore, that acquisition of good-quality spectroscopic data by conventional and laser-based methods should advance more rapidly, if progress in this field is not to be held up.

E. Scope of this Review

Some important spectroscopic aspects of quantum-resolved dynamics experiments have been summarized above. In particular, the relationship of radiative lifetime to other measures of the probability of an electronic transition has been discussed briefly.

In the experimental section, techniques for obtaining tunable radiation from pulsed dye lasers are reviewed, with particular reference to narrow-band lasers. The importance of narrow-band lasers in the present context lies in the possibility of selectively exciting resolved ro-vibrational states of electronically excited molecules, using the lasers. Methods for obtaining tunable ultraviolet radiation are also discussed.

Following the experimental section, we present the results of selected studies of small molecules using laser-induced fluorescence. Both dynamical and spectroscopic results are considered.

II. EXPERIMENTAL ASPECTS: FREQUENCY AND BANDWIDTH CONTROL OF PULSED LASERS IN THE VISIBLE AND ULTRAVIOLET

A tunable laser makes possible the studies of the spectroscopy and kinetics of excited states described in this chapter. Although a number of different types of laser can be tuned, the wavelength range is usually very narrow (< 1 nm). The dye laser is unique in possessing broad-band, continuous tunability in the wavelength range from -300 nm to $-1\,\mu$m. The use of nonlinear techniques, such as second harmonic generation (SHG) and frequency mixing in suitable media, further extends this range of tunability to less than 200 nm in the ultraviolet. This section is concerned with the control of the frequency and the bandwidth in dye lasers.

A. Pulsed Tunable Dye Laser

The basic principles of dye laser operation were reviewed in detail by Schafer (1973) and a complete bibliography of all literature concerned with dye lasers published between 1966 and 1972 is also available (Magyar, 1974).

Since that time the development of dye lasers has proceeded very rapidly. The first really successful and widely used design for a pulsed dye laser was that of Hansch (1972) and is shown in Fig. 1. The essential features of this cavity are the high dispersion echelle grating wavelength selector and the inverted telescope for collimating and expanding the beam. Collimation increases the resolution of the grating since it reduces the angular spread of the fluorescence from the dye cell, and expansion increases the resolution since more lines of the grating are illuminated. The angular dispersion of a diffraction grating in a Littrow mount is given (Longhurst, 1973) by

$$\frac{d\theta}{d\lambda} = \frac{p}{d\cos\theta} = \frac{2\tan\theta}{\lambda}, \tag{2.1}$$

where p is the diffraction order, d is the groove spacing of the grating and θ is the angle of the diffracted beam. In these pulsed dye lasers, the excitation time is typically of the order of 10 ns, so that only a few light passes within the cavity are possible. As a result, the linewidth of the dye laser is not much less than the single-pass bandwidth of the cavity. The linewidth (FWHM) $\Delta\lambda$ of the spectral distribution of the output beam is given (Littman and Metcalf, 1978) by

$$\Delta\lambda/\lambda = 2(\pi l \sin\theta), \tag{2.2}$$

where λ is the wavelength, l is the width of the illuminated part of the grating and θ is the angle between the grating normal and the incident beam. For a typical dye laser at ~ 500 nm, the single-pass resolution is usually in the range 0·005–0·010 nm.

Although this design is very successful, the use of the telescope has some disadvantages. Exact alignment of the telescope on the cavity axis produces undesirable feedback caused by reflection at the lenses. The telescope must therefore be slightly misaligned (Hansch, 1972; Hnilo *et al.*, 1980) and the optimum position is difficult to find. Since beam expansion

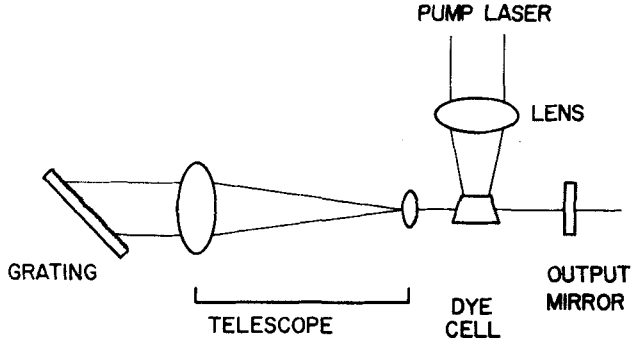

Fig. 1. Schematic diagram of a Hansch-type pulsed tunable dye laser.

is essential for narrow bandwidth operation of this type of dye laser cavity, a number of alternative types of beam expanders have been used. These include single- and multiple-prism devices (Myers, 1971; Stokes *et al.*, 1972; Hanna *et al.*, 1975; Nair, 1977; Klauminzer, 1977), reflective beam expanders (Eesley and Levenson, 1976; Beiting and Smith, 1979; Konig *et al.*, 1980; Hnilo *et al.*, 1980), and an arrangement whereby the expansion is realized directly by a grazing incidence upon the grating (Shoshan *et al.*, 1977; Littman and Metcalf, 1978; Littman, 1978; Saikan, 1978; Shoshan and Oppenheim, 1978; Dinev *et al.*, 1980; Godfrey *et al.*, 1980; Nair and Dasgupta, 1980).

The advantages of a prism beam expander are that magnification occurs in only one dimension, thus making it easier to align the grating, and they also allow the laser cavity to be shorter than with a telescope expander. Fig. 2 shows two different designs for a cavity utilizing a prism beam expander. In the single-prism arrangement (Hanna *et al.*, 1975; Stokes *et al.*, 1972), beam expansion is achieved by placing the prism at high angle of incidence (see Fig. 2(a)). The main disadvantages of this design are that the single-prism expander is not achromatic and there are high losses at the prism face. In

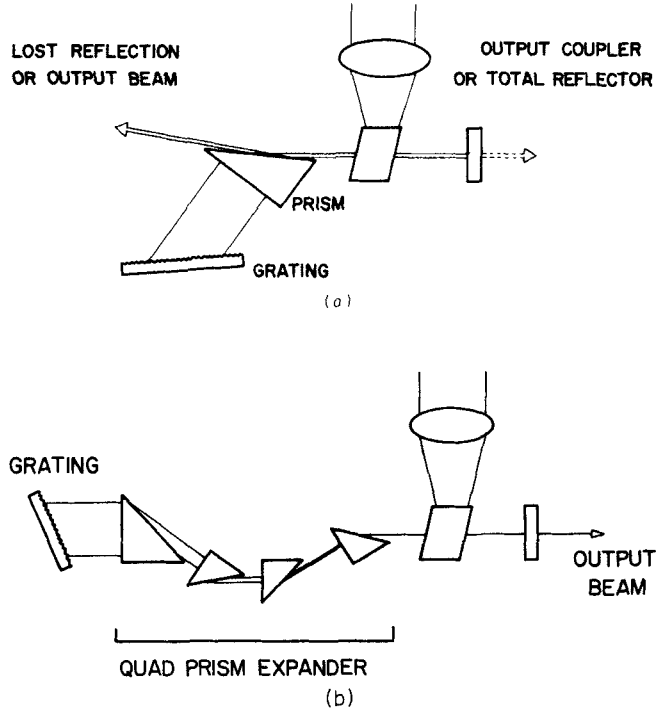

Fig. 2. Tunable dye laser cavities employing prism beam expanders. (a) Single-prism arrangement (Hanna *et al.*, 1975; Stokes *et al.*, 1972). (b) Quad-prism system (after Klauminzer, 1977).

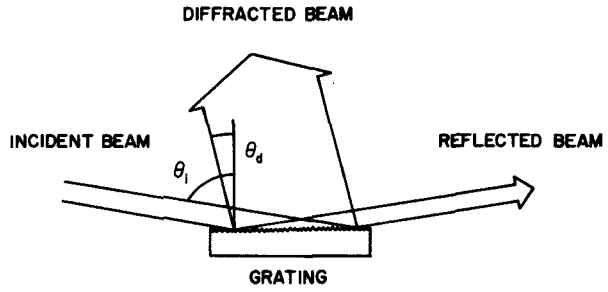

Fig. 3. Configuration for using a grating to expand a beam.

the multiple-prism expander described by Klauminzer (1977), four prisms at low angles of incidence, approaching Brewster's angle, are configured in achromatic pairs. This quad-prism system produced one-dimensional beam magnification of 40 × with high efficiency. Its only disadvantage is that the initial alignment of the prisms is difficult and high-quality coatings are required to reduce losses.

The most successful approach for replacing the telescope beam expander and reducing the cavity length is the use of gratings at large angles of incidence, usually in the range $89° \leqslant \theta_i \leqslant 90°$. Fig. 3 shows the arrangement and angles for a grating at grazing incidence. Beam expansion is achieved with the grating when the diffracted beam leaves the grating at an angle θ_d smaller than the angle of incidence θ_i. These angles are related by the standard grating equation (Longhurst, 1973)

$$\sin\theta_i + \sin\theta_d = p\lambda/d, \tag{2.3}$$

where d is the groove spacing, p is the diffraction order and λ is the wavelength. The magnification factor M is given by

$$M = \cos\theta_d/\cos\theta_i. \tag{2.4}$$

The value of M depends very strongly on the angle of incidence θ_i and a large magnification factor may be obtained as θ_i approaches 90°.

Demonstration of a dye laser using a grazing-incidence grating was made independently by Shoshan *et al.* (1977) and by Littman and Metcalf (1978). The designs of these two lasers differ slightly and are shown in Fig. 4. The tunning curve of these lasers is given (Littman, 1978) by

$$\lambda = d/p(\sin\theta_i + \sin\theta_d) \simeq d/p(1 + \sin\theta_d), \tag{2.5}$$

and the single-pass linewidth (FWHM) by

$$\frac{\Delta\lambda}{\lambda} = \frac{2(2\lambda)^{1/2}}{\pi l(\sin\theta_i + \sin\theta_d)} = \frac{2(2\lambda)^{1/2}}{\pi l(1 + \sin\theta_d)} \tag{2.6}$$

These equations can be compared with those for the Hansch-type dye laser

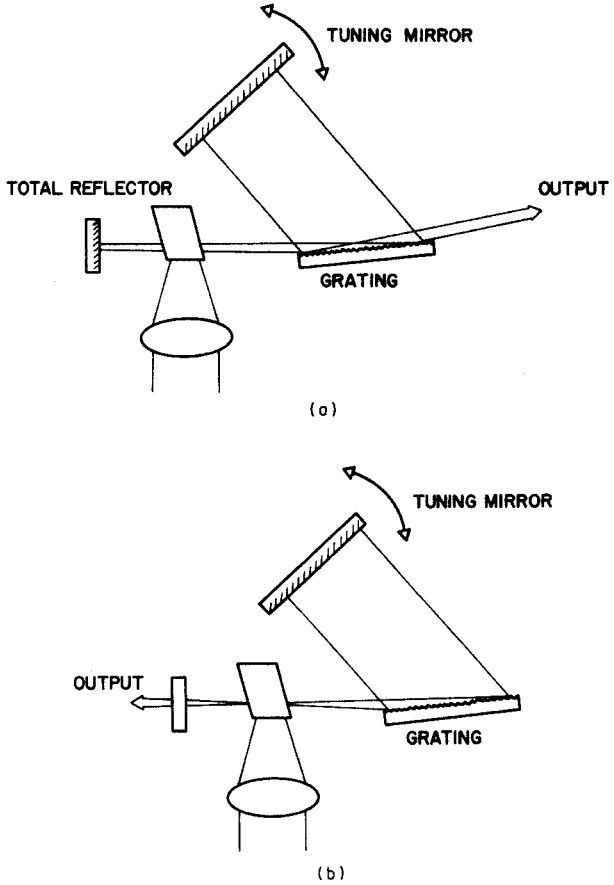

Fig. 4. Two configurations for a grazing-incidence grating dye laser. (a) After Shoshan *et al.* (1977). (b) After Littman and Metcalf (1978).

with the grating in a Littrow mount (Eq. (2.1) and (2.2)). The expression above predicts a linewidth about 30% less than for the Hansch laser.

Tuning of these lasers is controlled by the rotation of the tuning mirror. Rotation of the grating varies the magnification factor, and once the cavity is aligned the grating should remain fixed. The only limitation of this system is the small amount of feedback from the grating. However, the dye laser has sufficiently high gain to overcome this and, in principle, this method of tuning is applicable to any high-gain laser system.

B. Narrow Spectral Bandwidth Output

The dye lasers described above, comprising a grating and a beam expansion system, produce typical output linewidths of 0·2–0.5 cm^{-1}. For many

experiments a much narrower spectral linewidth is required, for example of the order of the Doppler width for spectroscopic experiments. Except for the grazing-incidence dye laser, this is normally achieved by placing a Fabry–Perot etalon inside the cavity in the collimated beam between the expander and the grating. Both solid and air-spaced etalons can be used, the only difference being the method used for tuning.

The etalon is constructed with two partially transmitting mirrors that are parallel to each other. When it is illuminated with a beam of coherent, monochromatic light, it will transmit the beam when the optical pathlength between the surfaces is an integral number of half-wavelengths of the incident light. This condition then defines the free spectral range (FSR) of the etalon as the spacing between successive transmission peaks

$$\text{FSR} = \begin{cases} \lambda^2/2nd & \text{(wavelength)} \quad (2.7a) \\ 1/2nd & \text{(wavenumber)} \quad (2.7b) \end{cases}$$

where d is the separation between the mirrors and n is the refractive index of the medium between the mirrors. The bandpass of the etalon depends on the finesse F, which is governed by a number of parameters: mirror parallelism, reflectivity, surface flatness, and scattering losses. The bandpass is given simply by the free spectral range divided by the finesse (FSR/F).

For use in the laser cavity, the etalon is chosen to have a free spectral range of about twice the linewidth of the laser without the etalon installed. This avoids overlapping of orders which would cause the laser to operate at a number of wavelengths (multimode) separated by the free spectral range. Thus an FSR of about 1 cm^{-1} is suitable for dye lasers of the types discussed above. A typical value for the finesse would be approximately 20, which leads to a single-pass linewidth of 0·05 cm^{-1}.

The etalon transmission maximum and the maximum of the spectral profile from the grating must be synchronized before the system can be used. This can be achieved either by tilting the etalon, which shifts the position of the transmission maximum, or by tilting the grating to shift the position of the maximum of the grating profile. This synchronization must be maintained at all times and thus there are special requirements if the laser wavelength is to be scanned. The scanning techniques for air-spaced and solid etalons are different.

A solid etalon is mounted in an adjustable kinematic holder and wavelength tuning is achieved by changing the tilt angle θ. For a solid quartz etalon such as is commonly used, the wavelength change, for a given order, as the etalon is rotated through an angle $\mathrm{d}\theta$ is given by

$$\mathrm{d}\lambda = -\lambda_0 \theta \, \mathrm{d}\theta / 2n_{\mathrm{d}}, \quad (2.8)$$

where n is the refractive index of quartz at wavelength λ_0, θ is the angle of rotation from the normal and λ_0 is the laser wavelength at $\theta = 0$. The

dispersive index n_d is given by

$$n_d = n - \lambda_0 \left| \frac{dn}{d\lambda} \right|. \tag{2.9}$$

Thus there is no simple relationship between the scanning of the grating, a sine function, and the scanning of the etalon. In order to scan any significant range of wavelength, it is necessary to use a computer to control the angles of the grating and the etalon.

Scanning can be somewhat simplified by using an air-spaced etalon. Both the etalon and the grating are enclosed in a pressure vessel and the wavelength is changed by varying the refractive index by changing the pressure of the gas in the pressure vessel (Wallenstein and Hansch, 1974, 1975). The wavelengths selected by both the grating and the etalon vary linearly with n. From a knowledge of the refractive index under ambient conditions, which can readily be calculated from its value at STP, and also the dye laser wavelength under these conditions, the wavelength at any pressure can be calculated from

$$\lambda = \frac{\lambda_A}{n_A} l + (n_A - 1)\frac{P}{P_A} \tag{2.10}$$

where λ is the output wavelength, P_A is the local ambient pressure, n_A is the refractive index and λ_A the output wavelength at P_A, and P is the pressure in the etalon/grating chamber. For a pressure change of 1 atm, the change in output wavelength is given by

$$\Delta\lambda = \lambda(n - 1) \qquad \text{(wavelength)}, \tag{2.11a}$$

or

$$\Delta\nu = -\nu(n - 1) \qquad \text{(wavenumber)}. \tag{2.11b}$$

Thus for two typical scan gases, $N_2 (n = 1{\cdot}000\,299)$ and $SF_6 (n = 1{\cdot}000\,783)$, the scan range for a 1 atm change is $4{\cdot}98\ \text{cm}^{-1}$ and $13{\cdot}05\ \text{cm}^{-1}$ respectively, or at 600 nm, 0·179 nm and 0·470 nm. High-pressure systems have been built in which pressure scans of up to 5 nm can be achieved (P. Hargis, 1980, private communication).

Several methods have been used to narrow the output linewidth in grazing-incidence grating dye lasers. For example, Saikan (1978) has replaced the total reflector with a resonant reflector and used the zero-order reflection to couple out of the cavity. In a laser designed to operate narrow-band simultaneously at two wavelengths, Dinev *et al.* (1980) used multiple-element resonant reflectors in place of the tuning mirror. Perhaps the most interesting method (Shoshan and Oppenheim, 1978; Littman, 1978) is the use of a second grating in a Littrow mount in place of the tuning mirror. Two possible orientations of the second grating satisfy the Littrow condition and they are shown in Fig. 5. However, only one orientation (full line in Fig. 5) can be

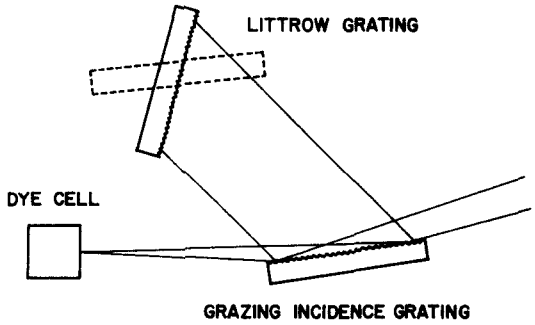

Fig. 5. Dual-grating, single-mode, pulsed tunable dye laser.

used since, for best operation, the dispersion of the grazing-incidence grating and the Littrow grating should be additive. The derivation of the tuning curves and single-pass linewidth of the double-grating system is complex and the reader is referred to the original papers of Shoshan and Oppeheim (1978) and Littman (1978). Since the wavelength is not a simple function of the grating rotation, the best method for continuous scanning is again pressure tuning. In operation, a laser of this design had a measured linewidth of about 750 MHz (0·025 cm^{-1}), but this was limited by jitter and the single-shot linewidth was estimated to be about 300 MHz (0·01 cm^{-1}) (Littman, 1978).

C. Oscillator–Amplifier Systems

The high-resolution dye laser oscillators described so far are not very efficient because of the losses associated with the intracavity dispersive optics. To obtain high output powers, a powerful pump laser can be used, but the risk of damage to optical elements in the cavity is increased. A more efficient method is to divide the pump laser beam and use some of its energy to drive a dye cell amplifier. Depending on the output power required, several stages of amplification may be employed (Wallenstein and Zacharias, 1980). Fig. 6 shows a diagram of an N_2-laser-pumped dye laser with two stages of amplification (Wallenstein and Hansch, 1975).

The influence of superfluorescence in oscillator–amplifier systems must be considered since it can compete with the external signal amplification, thus decreasing the overall efficiency. Several investigations of laser–dye amplifier systems have been published for both transversely pumped (Bonch-Breuvich *et al.*, 1975a, b; Ganiel *et al.*, 1975) and longitudinally pumped (Carlsten and McIlrath, 1973; Moriarty *et al.*, 1976; Narovlyanskaya and Tihkonov, 1978) arrangements. It has been shown that superfluorescence restricts the efficiency of conversion of pump laser energy into a useful signal when the injected signal is small. When the external signal is increased, the influence of the

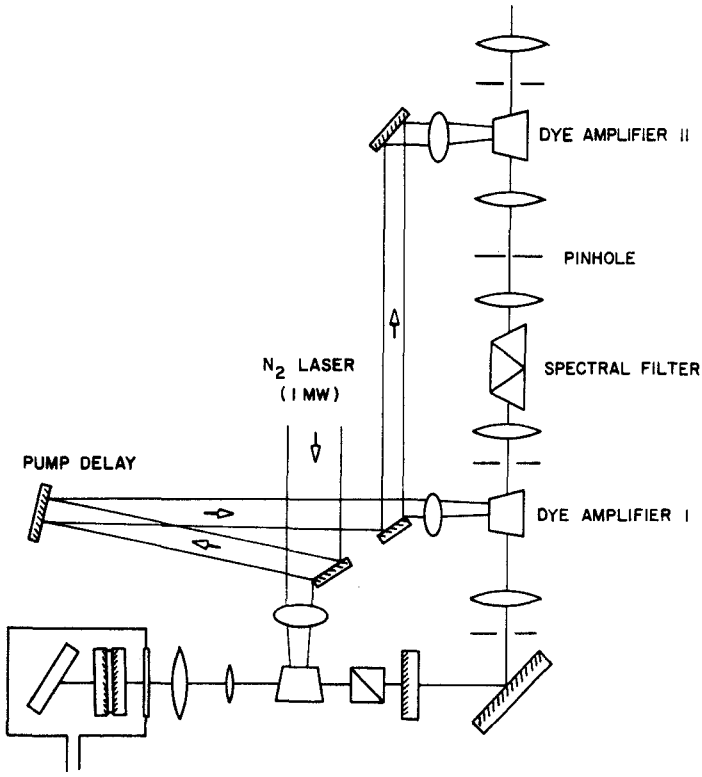

Fig. 6. Oscillator–amplifier dye laser system. Note the use of spectral and spatial filters between the amplifier stages to reduce the background of broadband spontaneous emission. After Wallenstein and Hansch (1975).

superfluorescence diminishes and the conversion efficiency increases. However, when the injected signal is very large, the efficiency is restricted as a result of saturation of the dye amplifier. Therefore the partitioning of the pump laser energy between oscillator and amplifier must be carefully judged.

D. Pump Sources

Little has been mentioned so far regarding suitable pump lasers for these dye lasers. Most of the lasers discussed above were originally designed to be pumped by nitrogen lasers at 337 nm in the ultraviolet. Even though the nitrogen laser proved to be a good pump laser, its peak power is limited to about 1 MW, or about 10 mJ per pulse maximum energy, which in turn limits the maximum energy available from the dye laser. Several other lasers have been found to be good dye laser pump sources. The most frequently used

TABLE I. Output characteristics of a typical neodymium:YAG laser[a] used to pump a dye laser.

Wavelength	Pulsewidth	Oscillator only		Oscillator–amplifier	
(nm)	(ns)	mJ/pulse	Peak power (MW)	mJ/pulse	Peak power (MW)
1064	8–9	225	25	700	80
532	6–7	70	10	225	32
355	5–6	40	6	125	20
266	4–5	20	4	60	12

[a] Quanta-Ray model DCR Nd:YAG laser.

alternative is the neodymium:YAG laser. The primary wavelength of the Nd:YAG laser, 1064 nm, cannot be used directly to pump a dye, but because of the high peak powers available this radiation can be converted efficiently to shorter wavelengths by nonlinear harmonic generation. The second, third and fourth harmonics of the Nd:YAG laser at 532, 355 and 266 nm, respectively, are all useful for pumping dyes. Similar to the dye lasers described earlier, the Nd:YAG laser can be operated in an oscillator–amplifier configuration which significantly increases the output power and the efficiency of harmonic generation. The output characteristics of a typical Nd:YAG laser used to pump dye lasers are given in Table I.

When the 532 nm radiation is used to pump a dye laser, overall dye laser efficiencies of greater than about 30% can be achieved at wavelengths longer than 540 nm. When the UV harmonics are used, the output efficiencies fall to approximately 20%. The tuning ranges of laser dyes vary with the pump laser wavelength, and the efficiency is usually highest when the fluorescence wavelength is close to the excitation wavelength. There are several studies of the tuning ranges of various dyes when pumped by the different harmonics of the Nd:YAG laser. For example, Ziegler and Hudson (1980) have measured the power tuning curves for several dyes in the range 333–390 nm when pumped with 266 nm radiation and Guthals and Nibler (1979) have published similar curves for 355 nm pumped laser dyes in range 410–715 nm.

The excimer lasers, particularly KrF at 248 nm (Sutton and Capelle, 1976; Rulliere *et al.*, 1977; Tomin *et al.*, 1978, 1979) and XeCl at 308 nm (Corney *et al.*, 1979; Uchino *et al.*, 1979; Huffer *et al.*, 1980) have also proved to be good pump sources. XeCl is perhaps the better of these sources since it has a long static fill lifetime; also its emission wavelength is more suited to pump a wide range of dyes thoughout the wavelength 340–710 nm. Typical output pulse energies of commercial excimer lasers are in the range 0·1–0·5 J and these units can operate at repetition rates up to 100 Hz. The peak powers

available with excimer laser pumping are typically two orders of magnitude greater than with N_2-laser excitation. The availability of these short-wavelength sources has stimulated the search for better short-wavelength dyes and it is now possible to obtain lasing with good efficiency down to 320 nm.

E. Frequency Doubling and Mixing

The range of useful laser output of a tunable dye laser can be extended well into the ultraviolet through the nonlinear optical techniques of frequency doubling and frequency mixing. Efficient SHG frequency conversion requires phase matching between the fundamental wave and its second harmonic. This can be obtained by properly adjusting the angle between the optical axis of the crystal and the input beam (Bloembergen, 1965; Terhune and Maker, 1968). The UV frequency can be continuously tuned by varying this angle.

There are a number of crystals which have the necessary optical properties for these nonlinear techniques. The four most frequently used are ammonium dihydrogen phosphate (ADP) (Dunning *et al.*, 1972), lithium formate monohydrate (LFM) (Dunning *et al.*, 1973), potassium dihydrogen phosphate (KDP) (Johnson and Swagel, 1971), and potassium pentaborate (KPB) (Dewey *et al.*, 1975; Dewey, 1976). The latter two crystals, KDP and KPB, can be used to cover the entire range from 217·3 to about 450 nm. Fig. 7 shows a series of tuning curves demonstrating how these crystals can be angle tuned to provide continuous output in this range. The efficiency of frequency doubling is dependent on beam quality, power, and wavelength. The highest efficiency ($\sim 10\%$) is obtained with KDP in the range 260–310 nm. The efficiency of KPB is considerably lower, 0·5–5% for the same input power.

In a scanning system it is necessary to maintain the correct phase-matched angle as the wavelength changes according to tuning curves, such as in Fig. 7. Several methods have been used to automate this procedure. Since the proper tilting angles of a grating and a crystal are different nonlinear functions of the wavelength, mechanical coupling of the two motions is difficult to achieve. One of the most elegant approaches was first developed by Kuhl and Spitschan (1975) who utilized the fact that, when the crystal is slightly misaligned, UV output can still be obtained but the direction of the UV beam is shifted. A similar but not identical technique has also been described by Bjorklund and Storz (1978). Two photodiodes were used to detect the spatial position of the UV beam. If the fundamental and harmonic beam spots are observed in a plane some distance from the SHG crystal, one would observe, as the crystal is rotated through the phase-matching angle, that the harmonic spot undergoes a displacement and grows in intensity as it approaches the fundamental spot and then fades again after passing through it. These diodes were then incorporated into a servo-feedback circuit so that

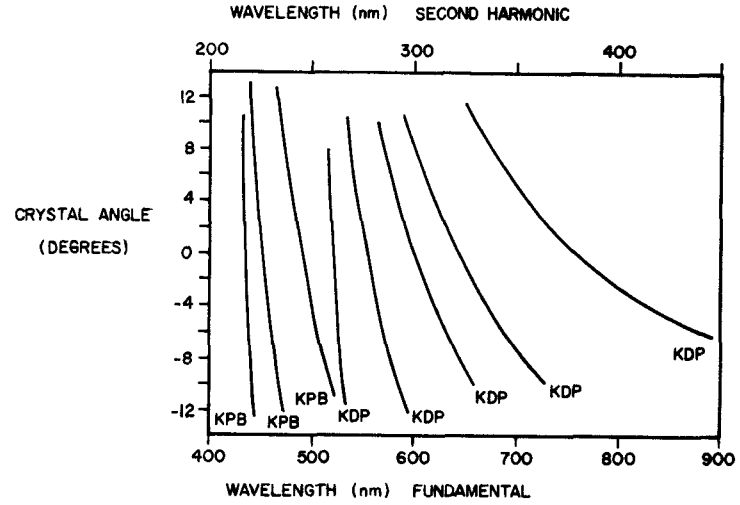

Fig. 7. Typical tuning curves, crystal angle versus wavelength, for correct phase matching of the fundamental and second harmonic beams in KDP and KPB.

any deviation of the UV output was automatically corrected by changing the tilt of the crystal.

Another method of automatic scanning can be used if a microprocessor is available to control the grating and crystal tilts. The tuning curves of the crystal can be determined experimentally and then fitted to some polynomical function. The coefficients of the fit can be stored in the computer and used to calculate the correct crystal angle at any wavelength. A motor and encoder can then be used to rotate the crystal to the correct angle.

Saikan (1976) and Saikan *et al.* (1979) have described a complicated system in which the frequency-doubling crystal remains fixed. The phase matching is achieved by changing the angle of the laser beam incident on the SHG crystal using dispersive components such as gratings and prisms. This system has been successfully used with KDP and LFM crystals.

Wavelengths shorter than 217 nm, which is the lowest limit for SHG, can be generated by sum frequency mixing (Dunning and Stickel, 1976; Kato, 1977a, b). Efficient sum frequency mixing of radiation at wavelengths λ_1 and λ_2, to produce radiation at wavelength λ_3, occurs when the phase-matching condition

$$\frac{n(\lambda_3)}{\lambda_3} = \frac{n(\lambda_1)}{\lambda_1} + \frac{n(\lambda_2)}{\lambda_2} \tag{2.12}$$

is satisfied, where

$$\frac{1}{\lambda_3} = \frac{1}{\lambda_1} + \frac{1}{\lambda_2} \tag{2.13}$$

and $n(\lambda)$ is the appropriate refractive index (Zernicke and Midwinter, 1973). By mixing, in KPB, the outputs of two tunable dye lasers, one operating in the infrared and one in the ultraviolet, Stickel and Dunning (1978) have obtained tunable radiation at wavelengths down to 185 nm.

In addition to providing shorter wavelengths than available from SHG, sum frequency mixing can also be used to generate higher-power radiation in the wavelength region where frequency doubling can be used. For example, megawatt power levels were generated by Stickel and Dunning (1978) in the range 240–248 nm by mixing the second harmonic of a ruby laser with the output of an infrared dye laser. The dye laser was pumped by the fundamental of the ruby laser. Similar schemes can be realized with the harmonics of a Nd:YAG laser.

The generation of tunable coherent vacuum ultraviolet (VUV) radiation has also been demonstrated (Mahon and Coopman, 1978; Wallenstein and Zacharias, 1980) using non-resonant frequency tripling in krypton gas. The rare gases exhibit only a small non-resonant third-order susceptibility and therefore efficient frequency tripling requires laser pulses of at least megawatt peak power. Using a pressure-tuned narrow-band dye laser with three amplifier stages and pumped by the second or third harmonics of a Nd:YAG laser, Wallenstein and Zacharias (1980) generated tunable light pulses at the Lyman-α wavelength (121·6 nm). With fundamental peak powers up to 9 MW and a bandwidth of more than $9 \times 10^{-3}\,\mathrm{cm}^{-1}$, the dye laser output at 364·6 nm was frequency tripled to give radiation at 121·6 nm with peak powers above 2 W and a bandwidth of $5{\cdot}2 \times 10^{-2}\,\mathrm{cm}^{-1}$. This method can be used for the generation of narrow-band VUV in several spectral regions between 105 nm, the transmission limit of LiF, and 147 nm, the lowest resonance line of xenon, in which the rare gases Kr and Xe exhibit negative dispersion.

F. Stimulated Raman Scattering

It is only very recently that stimulated Raman scattering (SRS) has found widespread use as a method of frequency conversion (Byer, 1980; Paisner and Hargrove, 1979). Efficient SRS is now possible because of the availability of high peak-power laser sources and the technique can be used to generate tunable radiation covering the electromagnetic spectrum from less than 200 nm to more than 1 μm.

In the SRS process, the pump laser pulse at frequency ν_P is incident on the scattering molecule which is in an initial state i, and can promote it to a virtual state. If sufficient transitions to this virtual level are induced, a population inversion can be generated between this virtual level and a final level f. Using the hydrogen molecule as an example, the initial state is the ground vibrational level and the final state is the first vibrational level. Stimulated emission then occurs at longer wavelength corresponding to the

frequency

$$\nu_P - (\nu_f - \nu_i) = \nu_P - \nu_R.$$

For hydrogen, the Raman frequency ν_R, is simply the fundamental vibrational frequency which is equivalent to 4155 cm^{-1}. The pump laser light converted in this process produces the first Stokes radiation (S_1) output.

As in a conventional laser scheme, there is an energy threshold below which no S_1 radiation is generated. Once above threshold, S_1 radiation increases exponentially in intensity as the pump intensity increases. Thus two intense waves, the pump and the S_1, propagate in phase through the gas and these waves harmonically beat against one another to produce a high-frequency sideband on the light. This conversion of light to a higher frequency ($\nu_P + \nu_R$) is called the first anti-Stokes radiation, AS_1. This process has no threshold once S_1 radiation appears. Higher-order anti-Stokes frequencies ($\nu_P + n\nu_R$) are produced in an equivalent manner and parametric generation of higher-order Stokes frequencies also occurs.

The three most commonly used gases are H_2, D_2 and CH_4 for which the shift increments are 4155 cm^{-1}, 2987 cm^{-1} and 2917 cm^{-1} respectively. Using a Nd:YAG pumped tunable dye laser which produced 20 mJ, 5 ns pulses at 560 nm, Paisner and Hargrove (1979) reported observation of transitions AS_8(195·7 nm) to S_2(1048 nm). With 208 nm radiation, they observed AS_4 (191.7 nm) to S_6(927.9 nm). With high output powers available from commercial dye lasers, spectral coverage in the UV can be achieved to below 175 nm

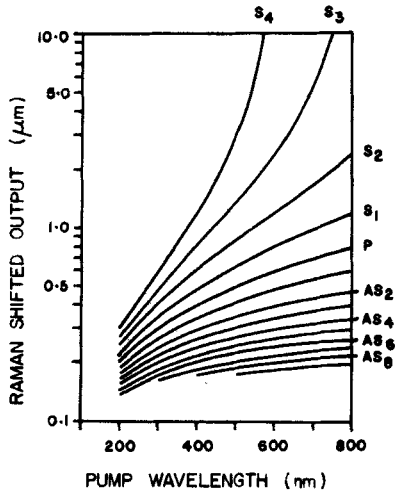

Fig. 8. Theoretical stimulated Raman scattering (SRS) wavelengths in H_2 (Quanta-Ray Corp).

using SRS with only a few dyes. In fact, this tuning range can be covered almost entirely using a rhodamine-6G dye laser alone.

To demonstrate the application of the technique of SRS, Paisner and Hargrove (1979) used the AS_7 component of the output of a rhodamine-6G dye laser to excite nitric oxide (NO). They obtained high-quality, high-resolution photoacoustic absorption spectra over the wavelength range 200–228 nm for the A–X system of NO.

A commercial SRS wavelength conversion accessory is now available (Quanta-Ray). With this system, eight orders of anti-Stokes and five orders of Stokes wavelengths have been observed. By varying the gas pressure, typically in the range 100–300 psi, the output in a particular line can be optimized. Although the highest energies are produced in the first few Stokes and anti-Stokes components, useful energies are obtained for relatively high-order conversions. Fig. 8 shows the theoretical SRS tuning curves using H_2 as the scattering gas.

III. LASER-INDUCED FLUORESCENCE STUDIES OF THE DIATOMIC HALOGENS AND INTERHALOGENS

The low-lying electronic states of the diatomic halogens and interhalogens give rise to banded (except F_2) and continuous absorption spectra in the visible and ultraviolet regions. The spectroscopy of the transitions involved is well understood and was the subject of two useful reviews (Coxon, 1973; Child and Bernstein, 1973). The states giving rise to these transitions are the ground state $X^1\Sigma_g^+$ (the g, u symmetry property is relevant only for the homonuclear molecules); the first excited state $A^3\Pi(1_u)$, which also correlates with ground-state atoms; the $B^3\Pi(0_u^+)$ state, which lies at only slightly higher energy than the A state and which correlates with one spin–orbit excited atom and one ground-state atom. There are then two repulsive states, $^1\Pi(1_u)$ and $Y0_g^+$; the $^1\Pi(1_u)$ state gives rise to the continuous absorption in the homonuclear halogens and the $Y0^+$ state is responsible for the predissociation of the B states in the heteronuclear interhalogens. Because they have opposite symmetry properties, the $Y0_g^+$ state is allowed to cross the $B^3\Pi(0_u^+)$ state in the homonuclear halogens without causing predissociation. Although the A and B states lie at similar energies above the ground state, thus causing the A–X and B–X systems to overlap, the spectra are easily differentiated since the A–X system contains one P, one Q and one R branch and the B–X only one P and one R branch.

Potential energy curves (Morse curves) for the low-lying states are shown in Fig. 9. The A state has not been observed for some of the molecules, namely Cl_2, ClF, BrCl, and is dubious for BrF. The A states are shown in Fig. 9 only when they are well known. The exact forms of the $Y0^+$ states are unknown although the crossing point with the B state can be estimated from

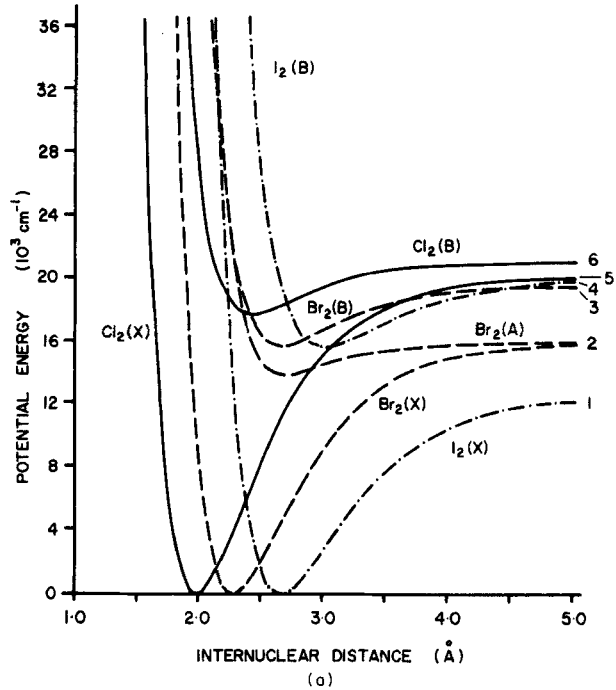
36
32
28
24
20
16
12
8
4
0
POTENTIAL ENERGY (10³ cm⁻¹)
I₂ (B)
Cl₂(B)
Br₂(B)
Cl₂(X)
Br₂(A)
Br₂(X)
I₂ (X)
6
5
4
3
2
1
1·0
2·0
3·0
4·0
5·0
INTERNUCLEAR DISTANCE (Å)

(a)

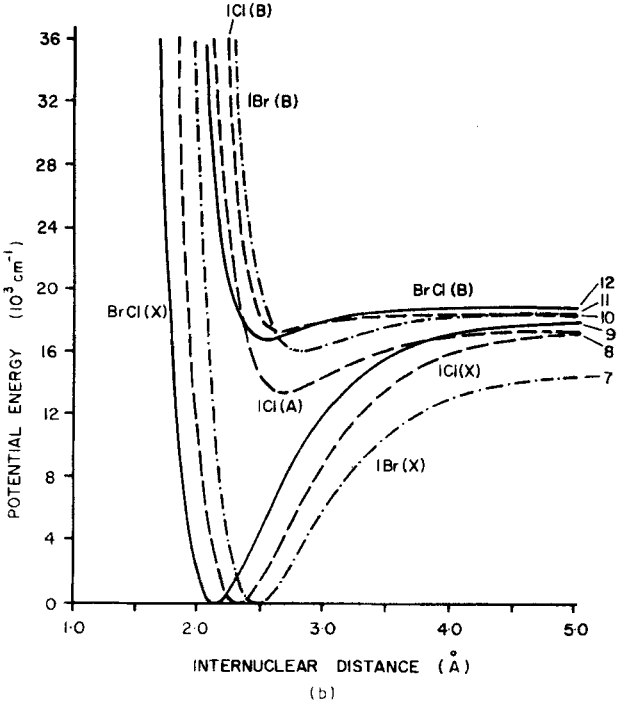
ICl (B)
IBr (B)
36
32
28
24
20
16
12
8
4
0
POTENTIAL ENERGY (10³ cm⁻¹)
BrCl (X)
BrCl (B)
ICl (A)
ICl(X)
IBr (X)
12
11
10
9
8
7
1·0
2·0
3·0
4·0
5·0
INTERNUCLEAR DISTANCE (Å)

(b)

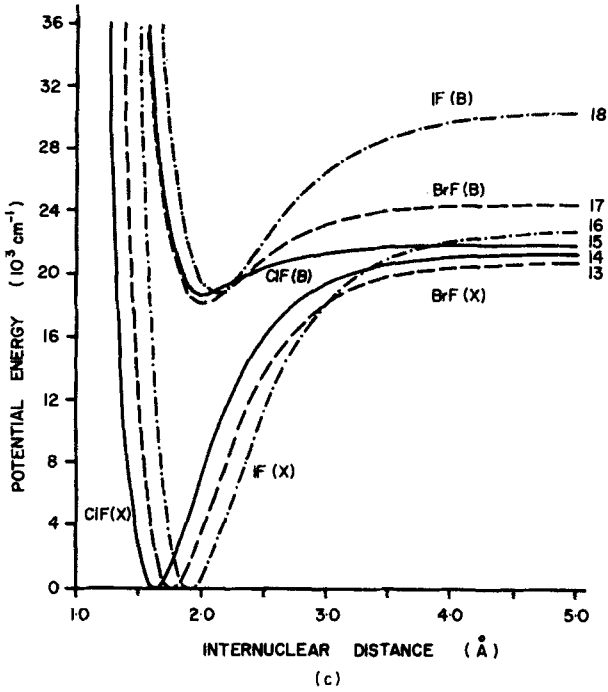

Fig. 9. Morse potential energy curves for the $B^3\Pi(0^+)$, $X^1\Sigma^+$, and, where known, the $A^3\Pi(1)$ states of the halogens and interhalogens. (a) I_2, Br_2, Cl_2. (b) IBr, ICl, BrCl. (c) IF, BrF, ClF. Dissociation products: 1, $I\,^2P_{3/2} + I\,^2P_{3/2}$; 2, $Br\,^2P_{3/2} + Br\,^2P_{3/2}$; 3, $Br\,^2P_{1/2} + Br\,^2P_{3/2}$; 4, $I\,^2P_{1/2} + I\,^2P_{3/2}$; 5, $Cl\,^2P_{3/2} + Cl\,^2P_{3/2}$; 6, $Cl\,^2P_{1/2} + Cl\,^2P_{3/2}$; 7, $I\,^2P_{3/2} + Br\,^2P_{3/2}$; 8, $I\,^2P_{3/2} + Cl\,^2P_{3/2}$; 9, $Br\,^2P_{3/2} + Cl\,^2P_{3/2}$; 10, $I\,^2P_{3/2} + Cl\,^2P_{1/2}$; 11, $I\,^2P_{3/2} + Br\,^2P_{1/2}$; 12, $Br\,^2P_{3/2} + Cl\,^2P_{1/2}$; 13, $Br\,^2P_{3/2} + F\,^2P_{3/2}$; 14, $Cl\,^2P_{3/2} + F\,^2P_{3/2}$; 15, $Cl\,^2P_{3/2} + F\,^2P_{1/2}$; 16, $I\,^2P_{3/2} + F\,^2P_{3/2}$; 17, $Br\,^2P_{1/2} + F\,^2P_{1/2}$; 18, $I\,^2P_{1/2} + F\,^2P_{3/2}$.

observations of the predissociation and it is known that they correlate with ground-state atoms.

Since they all have discrete absorptions in the visible spectrum, which can readily be obtained with tunable dye lasers, the halogens and interhalogens provide an interesting group of molecules for study with these techniques. As discussed in the introduction, the types of information available from an LIF study include radiative lifetimes, collisional energy transfer rates, predissociation rates and, sometimes, improvements to the spectroscopic constants. Since there are a number of curve crossings, detailed quantum-resolved measurements of the dynamics of the excited state can provide much information on the interesting effects of these crossings. As a group, the low-lying states of the homonuclear and heteronuclear diatomic interhalogens

are probably the most studied and best understood of any similar group of molecules.

There is a great deal of new information since the reviews by Coxon (1973) and by Child and Bernstein (1973). It is impossible to list all of the measurements, e.g. the lifetimes of individual ro-vibronic states, in a review such as this. Also, since there are significant differences in the behaviour of the different molecules, it is hard to make generalizations and therefore each molecule will be discussed individually. Trends that are clearly due to the family relationship of this group of molecules will be discussed at the end of this section.

A. Iodine, I_2

The extensive literature concerning the low-lying electronic states of iodine, up to 1973, has been reviewed by Coxon (1973). Wei and Tellinghuisen (1974) critically reviewed the available molecular constants of the $B^3\Pi(0_u^+)$ and $X^1\Sigma_g^+$ states of iodine in order to evaluate the best spectroscopic constants. Significant improvements to these constants have recently become available following the extension of Fourier transform spectroscopy to the study of electronic absorption and emission spectra of diatomic molecules in the near-infrared and visible regions. In a series of precise experiments, Gerstenkorn *et al.* (1977), Gerstenkorn and Luc (1978, 1979) and Luc (1980) have recorded and assigned some 14000 lines in 139 bands of the B–X system of I_2. New molecular constants and Dunham expansion parameters have been calculated from these data (Luc, 1980) for bands with $0 \leqslant v'' \leqslant 9$ and $1 \leqslant v' \leqslant 62$. Thus, the spectroscopic constants of the B–X system of I_2 are extremely well parametrized.

The resonance emissions of iodine, which can lead to spectroscopic information concerning the ground state, have long been the subject of many fluorescence studies (see, for example, Pringsheim, 1949). With the advent of lasers, the few transitions overlapping laser lines have been studied in more detail. Holzer *et al.* (1970a, b) observed fluorescence when iodine vapour was excited with the 514·5 and 501·7 nm lines of an Ar^+ laser, but they made no further analysis. The fluorescence from 514·5 nm excitation was investigated further by Ditman *et al.* (1975) and by Patterson *et al.* (1975). The experiments of these two groups were similar, and in both cases the fluorescence was excited by a narrow-bandwidth, single-frequency argon-ion laser and was resolved with a Fabry–Perot interferometer. Ditman *et al.* (1975) studied the emission line profile as the excitation wavelength was tuned through and away from resonance. They found that the intensity of the emission lines followed the absorption line profile whereas the frequency of the fluorescence was determined by the laser frequency. Patterson *et al.* (1975) studied the fluorescene spectrum when different modes of the argon-ion laser were used

to excite the iodine. In addition to the previously reported transitions (Halldorsson and Menke, 1970), 43–0 $R(15)$, 43–0 $P(13)$ and 58–1 $R(99)$, they observed three new transitions in the wings of the laser gain curve, 55–1 $P(87)$, 60–1 $P(103)$ and 44–0 $P(48)$. In order to assign the vibrational levels associated with the above transitions and to confirm the J' values obtained from the spectra, calculations of the energies were made using Wei and Tellinghuisen's (1974) constants. For the higher J' transitions, these energies were found to be in error by up to $1\,cm^{-1}$, although the agreement for lower J' was good. Most recently, Bacis *et al.* (1980) have recorded the I_2 fluorescence excited by the 514·5 and 501·7 nm Ar^+ laser lines using a high-resolution Fourier transform spectrometer. Spectra were obtained with both multimode and single-mode argon-ion lasers. With single-mode excitation, the fluorescence spectra exhibited a reduced Doppler width and spectra were recorded for $v'' = 10$–100. Broadening of quasibound $X^1\Sigma_g^+$ rotational levels above the rotationless $X^1\Sigma_g^+$ dissociation limit was observed and perturbations of the ground state, $v'' \geqslant 92$, by two previously unobserved long-range I_2 molecular states was detected. These two states, assigned as 0_g^+ and 1_g, which both correlate with two ground-state $I^2P_{3/2}$ atoms, were also observed directly in the fluorescence spectrum.

The measurement of lifetimes and self-quenching cross sections of levels in the $B^3\Pi(O_u^+)$ state of I_2 has been facilitated by the development of lasers. The first systematic studies, using direct observation of the fluorescence decay, by Sakurai *et al.* (1971) and by Capelle and Broida (1973), were restricted to the measurements of lifetimes associated with incompletely resolved vibrational bands. Vibrational bands of the B state were excited by a broad-band, 0.3–0.7 nm, dye laser. The results of Capelle and Broida (1973) provided a survey of the lifetimes and quenching cross sections for different vibrational levels. The lifetimes were found to be strongly dependent on v', varying from less than 0·4 μs to greater than 7 μs. Self-quenching cross sections showed less v' dependence, varying between 47 and 90 $Å^2$. Three peaks in the value of $1/\tau_{NR}$ were found at different excitation wavelengths. Near the dissociation limit, this increase in $1/\tau_{NR}$ was attributed to an increase in the radiative decay rate due to infrared emission to repulsive states, the most likely being 0_g^+ (Le Roy, 1970). The other peaks, at 550 nm and $\geqslant 620$ nm, were explained as being due to spontaneous predissociation by the repulsive $^1\Pi(1_u)$ state.

The lifetime of I_2 B state levels excited by transitions coincident with Ar^+ and Kr^+ laser lines were measured by Paisner and Wallenstein (1974). Their results agreed well with previous measurements. Sakurai *et al.* (1976) have considered the effects of narrow-bandwidth detection as well as narrow-band excitation. Lifetimes of two single rotational levels of $I_2(B)$ were measured with both vibrationally resolved (1.0 nm) and rotationally resolved (0.015 nm) detection. Measured radiative lifetimes were consistent with previous

measurements except that a 10% shorter lifetime was observed with single rotational line detection. The detector bandwidth dependence of the self-quenching cross sections were also measured by Sakurai *et al.* (1976). When all fluorescence is detected, the cross section refers to the average electronic quenching of the excited state and for initial excitation to $v' = 43$ the cross section $\sigma = 64 \text{Å}^2$. When the fluorescence from the originally excited level and also the rotational levels populated by relaxation are detected, the measured cross section is due to both electronic and vibrational relaxation and $\sigma = 76 \text{Å}^2$. For detection of just a single rotational transition, the cross section is due to the combined effects of electronic, vibrational, and rotational relaxation and $\sigma = 89 \text{Å}^2$.

TABLE II. Summary of lifetime measurements of $I_2(B)$ as a function of v' and J'. The cross section σ for destruction of the excited-state population is also given. After Broyer *et al.* (1975)

Excited levels				
v''	J'	τ_0(ns)	$1/\tau_0(10^6 \text{ s}^{-1})$	$\sigma(\text{Å}^2)$
20	40	890 ± 50	1·12 ± 0·06	65·5 ± 4
19	96	920 ± 40	1·09 ± 0·04	66·5 ± 3
18	37	970 ± 35	1·03 ± 0·04	70·5 ± 3
	58	955 ± 35	1·05 ± 0·04	69·2 ± 3
	85	968 ± 35	1·03 ± 0·04	68 ± 3
	104	977 ± 35	1·02 ± 0·04	69 ± 3
17	27	1146 ± 40	0·87 ± 0·03	66 ± 3
16	57	1227 ± 50	0·815 ± 0·03	61·9 ± 3
15	63	1356 ± 60	0·737 ± 0·03	63·7 ± 3
14	53	1314 ± 60	0·761 ± 0·03	63·9 ± 3
13	11	1260 ± 60	0·794 ± 0·04	65·2 ± 3
	73	1146 ± 50	0·873 ± 0·04	66·3 ± 3
12	32	1090 ± 50	0·917 ± 0·04	66·7 ± 3
	64	996 ± 40	1·004 ± 0·05	67·7 ± 3
	97	797 ± 40	1·255 ± 0·06	70 ± 3
11	8	920 ± 40	1·090 ± 0·05	71 ± 3
	76	701 ± 30	1·43 ± 0·06	72 ± 3
	90	605 ± 25	1·65 ± 0·07	71·5 ± 3
	102	565 ± 25	1·77 ± 0·08	73·5 ± 3
	112	478 ± 25	2·09 ± 0·1	72·5 ± 3
	126	390 ± 30	2·56 ± 0·2	68 ± 5
10	20	689 ± 30	1·45 ± 0·07	67·5 ± 3
	70	531 ± 25	1·88 ± 0·09	71·5 ± 3
	89	460 ± 25	2·17 ± 0·1	68·5 ± 3
9	33	596 ± 30	1·68 ± 0·9	69·5 ± 3
	39	569 ± 30	1·76 ± 0·9	72·5 ± 3
	61	480 ± 30	2·08 ± 0·12	73·5 ± 3
	84	380 ± 35	2·63 ± 0·25	76·5 ± 6

A number of experiments, of very different types, have proved that the $B^3\Pi(0_u^+)$ state suffers a weak natural predissociation (see, for example, Chutjian, 1969, and references therein). Vigue *et al.* (1974, 1975) have considered the data on the magnetic and natural predissociations of the B state of iodine. They have concluded that the same electronic state, the 1_u state, is responsible for both observations. They have also shown, from a theoretical standpoint, that the natural predissociation should be dependent on the magnitude of $J'(J'+1)$ according to

$$\Gamma_{\text{pred}} = k_{v'} J'(J'+1). \tag{3.1}$$

(We recall that the lifetime, $1/\tau_0 = \Gamma_{\text{rad}} + \Gamma_{\text{pred}}$.) In order to confirm their predictions, Broyer *et al.* (1975) measured the lifetimes of about 30 individual ro-vibrational levels. Table II summarizes their lifetime measurements. For $9 \leqslant v' \leqslant 13$ the lifetimes show a clear dependence on J'. The dependence of $k_{v'}$ on the vibrational energy is shown in Fig 10.

Predissociation of $I_2(B)$ to unbound states other than the $^1\Pi(1_u)$ has recently been studied by Sullivan and Dows (1980). Low-pressure I_2 vapour was excited to a vibrational state v' and the broad-band fluorescence was monitored. A modulated electric field was then applied which induced crossing from the B state to a dissociative state, thus causing a reduction and a modulation of the fluorescence intensity. The electric field can couple the $B^3\Pi(0_u^+)$ state to predicted, unbound 0_g^+ and 1_g^+ states. The dependence of the induced predissociation on v' was studied and the results indicated that an unbound state, probably the 0_g^+, crosses the B state near $v = 3$–4 on the outer limb. The transition dipole moment between the B and the unbound state was 0·03–0·04 D.

High vibrational levels of the $B^3\Pi(0_u^+)$ state near its dissociation limit and also highly excited electronic states in the 5 eV region have been studied in a series of elegant two-photon experiments by Danyluk and King (1976a, b, 1977a, b) and King *et al.* (1980). In single-photon electronic absorption spectra of heavy molecules such as iodine, the very high density of ro-vibrational

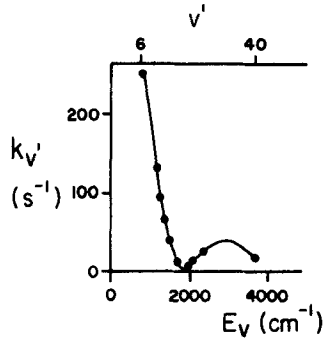

Fig. 10. $k_{v'}$ as a function of the vibrational energy E_v in the $B^3\Pi(0_u^+)$ state of I_2. The curve is just a rough interpolation between the experimental points. After Broyer *et al.* (1975).

states close to the dissociation energy produces a spectrum which is indistinguishable from the adjoining continuum. Single-photon laser excitation of I_2 B–X gives a complex, partially resolved spectrum from which the dissociation energy can be estimated directly to only $\pm 12\,cm^{-1}$ (Ornstein and Derr, 1976). Danyluk and King (1976a, 1977b) have used two-photon sequential absorption spectroscopy, in which the iodine molecule is first excited from the ground state to the B state and then to the higher E state. It was possible to excite selectively rotational band structure for the B–X system up to within $0{\cdot}5\,cm^{-1}$ of the dissociation limit. The amount of rotational structure observed depended on the ratio of the bandwidth of one of the exciting dye lasers to the rotational constant in the E state. This ratio could be varied to change the observed rotational line density and complexity. From their study using this technique under very high resolution, Danyluk and King (1977b) obtained and improved value for the dissociation limit of the $B^3\Pi(0_u^+)$ state, $D_0^0 = (20\,043{\cdot}063 \pm 0{\cdot}20)\,cm^{-1}$. The higher levels studied also allowed the determination of values for the constants C_5, C_6, and C_8 in the long-range potential out to an internuclear separation of 15 Å. Recently, King *et al.* (1980) have examined the analogous levels of $^{129}I_2$ by the same technique. Vibrational and rotational constants were obtained for B state levels with $v' = 71$–79 and the dissociation energy was measured to be $D_0^0(^{129}I_2) = 20\,043{\cdot}897\,cm^{-1}$. The results from studies of both $^{127}I_2$ and $^{129}I_2$ were combined to give improved values of the long-range constants of the B state.

The ground $X^1\Sigma_g^+$ state of iodine has gerade symmetry. Thus, excited states of even parity are not accessible by single-photon absorption from the ground state and very little is known about them. Danyluk and King (1976b, 1977a), using a similar technique to that described above, have excited iodine molecules first to the ungerade B state and then into levels of gerade excited electronic states in the energy range of 5·0–5·5 eV. Five vibrational progressions have been identified and analysed, and were labelled $\alpha, \beta, \gamma, \delta$, and ε. Vibrational and rotational constants were obtained for these five excited electronic states, which have ion-pair character. The symmetries of two of

TABLE III. Vibrational constants (cm^{-1}) for the $\alpha, \beta, \gamma, \delta$, and ε excited states of I_2. After Danyluk and King (1977a).

	T_e	ω_e	$\omega_e x_e$	$\omega_e y_e$
α	40281·8	104·83	0·324	$3{\cdot}9 \times 10^{-3}$
β	40925·1	104·07	0·219	$8{\cdot}6 \times 10^{-5}$
γ	41513·6	95·53	0·310	$6{\cdot}7 \times 10^{-3}$
δ	41682·9	100·41	0·180	—
ε	42493·7	95·75	0·0265	$-7{\cdot}4 \times 10^{-3}$

these states were identified as 0_g^+, and the other three as either 0_g^+ or 1_g^+. All five of the excited states have vibrational frequencies of the order of $100\,cm^{-1}$ and are summarized in Table III. The equilibrium internuclear distances are $r_e = 3{\cdot}676$ and $3{\cdot}513$ Å for the α and β states respectively.

B. Bromine, Br_2

The discrete region of the $B^3\Pi(0_u^+)$–$X^1\Sigma_g^+$ system of bromine extends from about 510 to 740 nm. Despite the simple P and R branch structure of these bands, the low magnitudes of the vibrational and rotational constants give rise to a strongly overlapped, dense spectrum. The complexity of the spectrum is enhanced by the natural occurrence of the three isotopic species $^{79}Br_2$, $^{79}Br^{81}Br$, $^{81}Br_2$ in the approximate ratio 1:2:1. The most comprehensive and accurate spectroscopic constants for the B–X system were obtained from a high-resolution absorption study on separated isotopes by Barrow *et al.* (1974). High-resolution data for $v'' > 10$ do not exist, but low-resolution observation of the UV resonance fluorescence spectrum by Rao and Venkateswarlu (1964) provided constants ($\pm 1\,cm^{-1}$) for v'' levels up to 36. Improved RKR curves for the B and X states were determined by Barrow *et al.* (1974) which confirmed the validity, for $v' \leqslant 19$, of the Franck–Condon factors calculated by Coxon (1972a).

Bromine is the only homonuclear interhalogen for which accurate data for the weaker $A^3\Pi(1_u)$–$X^1\Sigma_g^+$ transition have been obtained. This system extends from about 640 to 710 nm and is difficult to separate from the more intense, overlapping B–X system. However, high-resolution absorption spectra were recorded by Horsley (1967) and by Coxon (1972b). RKR curves for the A state and Franck–Condon factors for the A–X system were calculated by Coxon (1972c).

Laser-induced fluorescence on the B–X system of Br_2 was first reported by Holzer *et al.* (1970a, b). A progression of fluorescence doublets was observed following excitation with the 514·5 nm line from an argon-ion laser. From a comparison of the measured vibrational constants with those from absorption spectra, the emitting isotope was identified as $^{81}Br_2$. The doublet spacing gave a J' value of 15, and, although the vibrational level could not be defined accurately, it was thought to be close to $v' = 39$. This suggestion was later confirmed by Coxon (1973), based on the agreement between the relative band intensities of the fluorescence progression and the calculated Franck–Condon factors. More recently, Hozack *et al.* (1980) have reported a new study of LIF in Br_2, excited by a Kr^+ laser.

Coxon (1973) calculated a value for the radiative lifetimes of the B and A states of Br_2 using values of the electronic transition moment R_e, obtained from absorption spectral data. His estimates were $\sim 25\,\mu s$ for the B state lifetime and ~ 2 ms for the A state lifetime. The first measurements of the

radiative lifetime of the B state using laser-induced fluorescence techniques produced widely different values for τ_0. Capelle *et al.* (1971) used a dye laser with an output bandwidth of 1–8 Å to excite vibrational levels between $v' = 1$ and 31. Lifetimes and self-quenching cross sections were measured by observing directly the decay of fluorescence as a function of pressure. Large variations, by a factor of 8, in the lifetime were observed, ranging from more than 1·2 μs near $v' = 27$ to less than 0·15 μs near $v' = 14$. This variation was interpreted as due to spontaneous predissociation of the B state through dissociative states. However, Coxon (1973) has pointed out the uncertainty with these measurements owing to possible contamination by molecular iodine.

Zaraga *et al.* (1976) used narrow-linewidth excitation near 558 nm to populate specific ro-vibrational (v', J') states in $^{81}Br_2(B)$. From absolute absorption measurements, which permitted an accurate calculation of the electronic transition dipole moment, an estimate of 20 μs was made for the radiative lifetime of the B state. Actual fluorescence decay lifetimes at zero pressure were found to be much shorter than the radiative lifetime because of the effects of predissociation. Zero-pressure lifetimes of 0·11, 0·31 and 0·5 μs were measured for the levels (16,48), (19,40) and (23,46) respectively.

Several specific levels near the dissociation limit of $Br_2(B)$ were studied by McAfee and Hozack (1976). The lifetime was found to depend sharply on v' and J' and they reported lifetimes ranging from 3·57 to 1·57 μs for various levels with $40 \leqslant v' \leqslant 47$ and $16 \leqslant J' \leqslant 42$. The quenching cross sections were found to increase systematically, from 70 Å^2 for $v' = 40$ to 88 Å^2 for $v' = 46$ and 47, as the dissociation limit was approached. A more detailed study of this type has been reported recently by Luypaert *et al.* (1980). These workers report variations of lifetime with v' and J' that are consistent with heterogeneous predissociation of the B state (see below).

As for Cl_2 (see next section), the radiative lifetime of bromine trapped in solid argon has been measured (Bondybey *et al.*, 1976). In contrast with the chlorine case, excitation into the bound levels, or into the continuum of the $B^3\Pi(0_u^+)$ state of bromine isolated in a rare-gas matrix, resulted in emission from the $v' = 0$ level. Thus, there was fast vibrational relaxation but no radiationless transitions into other electronic states and no communication between the different components of the $^3\Pi$. The radiative lifetime was found to be 7·6 μs in argon, and 8·6 and 6·4 μs in neon and krypton respectively. Based on extrapolation, Bondybey *et al.* (1976) predicted a lifetime of (12 ± 2) μs for $v' = 0$ of the gas-phase molecules.

An extensive and systematic study of the laser excitation spectrum, radiative lifetimes, and quenching rate constants for both the $B^3\Pi(0_u^+)$ and $A^3\Pi(1_u)$ states of bromine has recently been made by Clyne and Heaven (1978) and Clyne *et al.* (1980b, c). Clyne and Heaven (1978) first reported the observation of the high-resolution laser excitation spectrum of the B–X system. The